The Astrophysical Journal Letters, 967:L22 (12pp), 2024 June 1 https://doi.org/10.3847/2041-8213/ad46fa

Chemical Diagnostics to Unveil Environments Enriched by First Stars

Irene Vanni[1,2], Stefania Salvadori[1,2], Valentina D'Odorico[3,4,5], George D. Becker[6], and Guido Cupani[3]
[1] Dipartimento di Fisica e Astrofisica, Università degli Studi di Firenze, Via G. Sansone 1, I-50019, Sesto Fiorentino, Italy; irene.vanni@unifi.it
[2] INAF/Osservatorio Astrofisico di Arcetri, Largo E. Fermi 5, I-50125, Firenze, Italy
[3] INAF/Osservatorio Astronomico di Trieste, Via G. Tiepolo 11, I-34143, Trieste, Italy
[4] Scuola Normale Superiore, Piazza dei Cavalieri 7, I-56126, Pisa, Italy
[5] IFPU—Institute for Fundamental Physics of the Universe, via Beirut 2, I-34151, Trieste, Italy
[6] Department of Physics & Astronomy, University of California, Riverside, CA-92521, USA
Received 2024 February 29; revised 2024 April 27; accepted 2024 May 2; published 2024 May 22

Abstract

Unveiling the chemical fingerprints of the first (Population III, hereafter Pop III) stars is crucial for indirectly studying their properties and probing their massive nature. In particular, very massive Pop III stars explode as energetic pair-instability supernovae (PISNe), allowing their chemical products to escape in the diffuse medium around galaxies, opening the possibility to observe their fingerprints in distant gas clouds. Recently, three $z > 6.3$ absorbers with abundances consistent with an enrichment from PISNe have been observed with JWST. In this Letter, we present novel chemical diagnostics to uncover environments mainly imprinted by PISNe. Furthermore, we revise the JWST low-resolution measurements by analyzing the publicly available high-resolution X-Shooter spectra for two of these systems. Our results reconcile the chemical abundances of these absorbers with those from literature, which are found to be consistent with an enrichment dominated (>50% metals) by normal Pop II SNe. We show the power of our novel diagnostics in isolating environments uniquely enriched by PISNe from those mainly polluted by other Pop III and Pop II SNe. When the subsequent enrichment from Pop II SNe is included, however, we find that the abundances of PISN-dominated environments partially overlap with those predominantly enriched by other Pop III and Pop II SNe. We dub these areas confusion regions. Yet, the odd–even abundance ratios [Mg,Si/Al] are extremely effective in pinpointing PISN-dominated environments and allowed us to uncover, for the first time, an absorber consistent with a combined enrichment by a PISN and another Pop III SN for all the six measured elements.

Unified Astronomy Thesaurus concepts: Chemical abundances (224); Abundance ratios (11); Population III stars (1285); Damped Lyα systems (349)

1. Introduction

Understanding the properties of the first (Population III, hereafter Pop III) stars and their impact on subsequent galaxy formation is a fundamental problem (e.g., Klessen & Glover 2023). Discovering the chemical fingerprints of Pop III stars exploding as supernovae (SNe) is crucial to achieve this goal (e.g., Koutsouridou et al. 2023). Indeed, cosmological simulations show that Pop III stars were more massive than present-day stars (e.g., Hirano et al. 2014; Susa et al. 2014), an idea also supported by the persistent lack of metal-free stars (e.g., Rossi et al. 2021). Thus, most Pop III stars might have rapidly disappeared as SNe, promptly enriching the pristine gas with their newly formed chemical products.

Pop III SNe with various progenitor masses and explosion energies synthesize different heavy elements (e.g., Heger & Woosley 2010; Kobayashi 2012), thus producing distinctive chemical fingerprints (see Vanni et al. 2023a). These unique signatures can be observed in distant gaseous absorbers directly enriched by these pristine sources (Saccardi et al. 2023), or in long-lived metal-poor stars born in Pop III–enriched environments (e.g., Frebel et al. 2019; Skúladóttir et al. 2021). Stellar evolution calculations for the chemical products of very massive pair-instability SNe (PISNe; $M_* = 140$–$260\,M_\odot$; Barkat et al. 1967) are extremely robust and predict unique abundance patterns, featuring a strong odd–even effect (Heger & Woosley 2002; Takahashi 2018).

Many efforts have been dedicated to seek out these unique PISN fingerprints (see Salvadori et al. 2019; Aguado et al. 2023; Caffau et al. 2023) and finally one possible pure PISN descendant has been found in the LAMOST survey (Xing et al. 2023). If predominantly enriched by PISN (see Jeena et al. 2024), this unique star will provide us with the first tight constraints on the initial mass function (IMF) of Pop III stars (Koutsouridou et al. 2024).

PISNe are very energetic ($E_{SN} \in [10^{52}; 10^{53}]$ erg); thus their metals can easily escape their hosting galaxies (e.g., Bromm et al. 2001; Smith et al. 2015) filling the diffuse circumgalactic and intergalactic media (e.g., Pallottini et al. 2014). Thus, the long-waited discovery of this PISN descendant opens the concrete possibility to pinpoint the chemical fingerprint of PISNe in high-z diffuse absorbers too. Very recently, Christensen et al. (2023) reported chemical abundances consistent with a PISN enrichment for three $z > 6.3$ absorbers observed in JWST QSO's spectra. Indeed, they found that these systems have high [Si/O] > 0.5 values and only upper limits for [C/O] < 0 (see, e.g., Ma et al. 2017a; D'Odorico et al. 2023a).

In this Letter, we aim at addressing the reliability of the JWST low-resolution measurements and the determination of the key abundance ratios that need to be measured in order to identify PISN-enriched environments. Our final goal is to

provide new chemical diagnostics to pinpoint distant absorbers predominantly enriched by PISNe and other Pop III SNe.

2. Summary of the Model

For this study, we use the model first introduced by Salvadori et al. (2019) and then generalized by Vanni et al. (2023b). This simple and general parametric study investigates the chemical abundances (elements from C to Zn) of gaseous environments imprinted by a single Pop III SN and subsequently polluted by normal (Pop II) SNe. Pop III stars are indeed expected to predominantly form in isolation in low-mass minihalos (e.g., Hirano et al. 2015). Furthermore, simulations show that in these protogalaxies self-enrichment from a single Pop III SN can promptly trigger the formation of normal Pop II stars by enriching the interstellar medium (ISM) above the critical metallicity value (e.g., Ritter et al. 2012). The model is quite robust since our findings for ancient metal-poor stars (Vanni et al. 2023b; Skúladóttir et al. 2024) have been confirmed by more sophisticated cosmological chemical evolution models and simulations (Koutsouridou et al. 2023; Rossi et al. 2023). The model was used to unveil the Pop III star's signature in distant gaseous absorbers (Salvadori et al. 2023; Sodini et al. 2024), which is a proof of its versatility.

The innovative aspects of our approach with respect to other simple models available in literature (e.g., Ishigaki et al. 2018; Welsh et al. 2019) are reported below.

A parametric study. The uncertainties related to early cosmic star formation are enclosed in two free parameters: the star formation efficiency, f_*, which quantifies the amount of cold gas turned into stars, and the dilution factor, $f_{\rm dil}$, which varies depending upon the amount of gas available to dilute metals. A third parameter, $f_{\rm PopIII}$, sets the fraction of metals in the ISM provided by Pop III with respect to Pop II SNe. The chemical abundances of the gas, [X/H], depend on the ratio $f_*/f_{\rm dil}$ and $f_{\rm PopIII}$ (see Vanni et al. 2023b), and thus are evaluated by varying these unknowns in the full parameter space: $f_*/f_{\rm dil} \in [10^{-4}; 10^{-1}]$ and $f_{\rm PopIII} \in [1,\ 0.01]$. Conversely, the relative abundance ratios of different chemical elements, $[X/Y]$, are strongly influenced by $f_{\rm PopIII}$ but they only indirectly depend on $f_*/f_{\rm dil}$, which sets the initial metallicity of subsequent generations of Pop II stars (see Salvadori et al. 2019).

Exploring the properties of Pop III SNe. To investigate the whole range of unknown properties of Pop III SNe, we exploit the tabulated yields of Heger & Woosley (2010), which represent the most complete data sets for Pop III SNe with progenitor masses between 10 and 100 $M_\odot$. Indeed, the authors investigate the chemical products of these SNe, that can potentially explode with different energies: from the lowest-energy *faint SNe*, $E_{\rm SN} = 0.6 \times 10^{51}$ erg, to the most energetic *hypernovae*, $E_{\rm SN} = 10^{52}$ erg, adopting different mixing parameters. Here we explore this full parameter space. For more-massive, $m_\star = 140$–$260\,M_\odot$, Pop III stars exploding as energetic PISNe, $E_{\rm SN} = 10^{52}$–10^{53} erg, we adopt the yields by Heger & Woosley (2002). For our exploration we are thus implicitly assuming that Pop III SNe with different progenitor mass within the range $m_\star = 10$–$100\,M_\odot$ and $m_\star = 140$–$260\,M_\odot$, and different SN explosion energies have an equal probability to explode. Note that considering a burst of Pop III SNe with the same mass/explosion energy instead of a single SN would not change the results. Finally, here we also investigate how the abundance ratios of PISNe-enriched environments change after the explosion of a second Pop III SN (see Appendix B).

Subsequent pollution by Pop II SNe. To study how the chemical abundances vary due to the further contribution of Pop II SNe, we assume that Pop II stars are distributed according to a Larson's IMF, $\phi(m_\star) \propto m_\star^{-2.35} \times \exp(-m_{\rm ch}/m_\star)$ with $m_{\rm ch} = 0.35\,M_\odot$ and compute the contribution of Pop II stars above different masses, which allow us to evaluate the effect of SNe evolving on different timescales (see Salvadori et al. 2019). For Pop II SNe, we adopt the recent yields from (Limongi & Chieffi 2018; nonrotating, set R).

3. Observational Data

Our compiled literature sample consists of 50 different metal-poor absorption systems analyzed in Cooke et al. (2011), Becker et al. (2012), Welsh et al. (2022), Saccardi et al. (2023; only with [Fe/H]$\leqslant -1$), and Christensen et al. (2023). The redshifts of the absorbers range between $\sim$2 (Cooke et al. 2011) and $\sim$7.5 (Christensen et al. 2023). These absorbers have different nature: 24 are Damped Lyα systems (DLAs; Cooke et al. 2011; Welsh et al. 2022) and 19 more diffuse sub-DLAs and Lyman Limit systems (Saccardi et al. 2023). The systems at $z \gtrsim 5$ (Becker et al. 2012; Christensen et al. 2023) were selected from the presence of the O I absorption, tracer of neutral gas, because the H I content is hardly measurable at these redshifts. Therefore, they are DLAs or sub-DLAs, but their precise nature is unknown. The main elements whose abundances can be measured are C, O, Mg, Al, Si, and Fe, but these elements are simultaneously available for nine absorbers only.

3.1. New Measurements

The analysis of the three systems with possible PISN enrichment by Christensen et al. (2023) have been carried out in JWST/NIRSpec spectra at low spectral resolution ($R \approx 2700$). Two of these systems fall in the spectra of the QSOs UHS J0439+1634 ($z_{\rm em} = 6.5185$) and ULAS J1342 +0928 ($z_{\rm em} = 7.5353$), respectively, which also have intermediate resolution ($R \approx 9000$) good signal-to-noise ratio VLT/X-Shooter data.

The X-Shooter spectrum of J0439+1634 was presented in D'Odorico et al. (2023b) and analyzed in Davies et al. (2023). However, these authors do not identify the O I 1302 Å transition associated with the system at $z = 6.2897$, discussed by Christensen et al. (2023), because it falls in a spectral region already populated by other absorption lines (see Davies et al. 2023, for details). Our analysis of the system is reported in Appendix A.

The analysis of the X-shooter absorption spectrum of J1342 +0928 is carried out in this work for the first time, and is described in Appendix A.

For the purpose of this Letter, we analyzed only the two O I absorption systems at $z = 7.369$ and $z = 7.443$ for which Christensen et al. (2023) reported the chemical abundances, the former showing possible PISN enrichment. However, we carried out a first look analysis of the whole spectrum to verify that the transitions of the considered systems were not blended with lines from other systems.

Observed absorption features were identified and fitted with Voigt profiles to determine ionic column densities. We derived chemical abundances from the ratio of the measured column

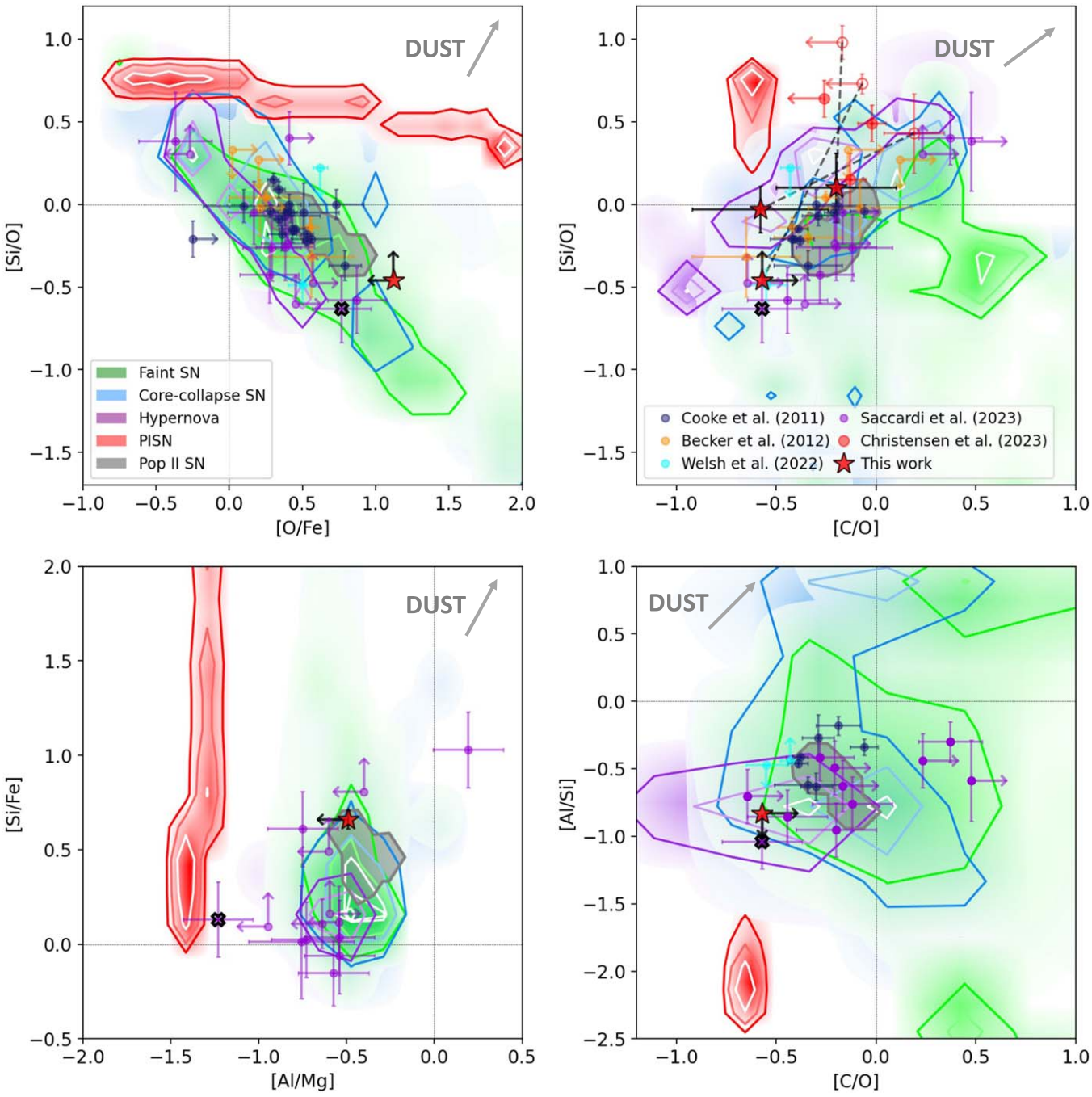

Figure 1. Chemical abundances predicted for environments uniquely enriched by PISNe (red), by other Pop III SNe (faint SNe: green; core-collapse SNe: blue; hypernovae: purple), and by normal Pop II SNe (gray shaded areas). Each environment is enriched by a single Pop III SN with different mass and explosion energy. The contours with decreasing color intensity identify 30%, 60%, and 90% probability densities, corresponding to the fraction of environments predicting those abundances for each SN type. Points with error bars are the measured abundances of absorbers in the literature (Section 3; labels). The values reported by Christensen et al. (2023; red empty) are connected with the new measurements obtained using higher-resolution spectra (star). The absorber in the sight line to J1018+0548 (Saccardi et al. 2023; $z = 3.39$) is highlighted with a black cross (see Section 4.2). The arrows show in which direction dust depletion would modify the predicted abundances.

densities and adopting solar chemical abundances from Asplund et al. (2009). Based on the common hypothesis that these systems are metal-poor DLAs (e.g., Becker et al. 2012; Christensen et al. 2023), we did not correct for ionization effects and dust depletion. Measured column densities and plots of the absorption lines are reported in Appendix A.

The abundances for the system in UHS J0439+1634 and the two systems in ULAS J1342+0928 as derived by Christensen et al. (2023) are shown in Figure 1 with red empty points. These points are connected with dashed black lines to the revised abundances derived in this work (red stars), which are reported in Table 1. The new abundances derived from X-Shooter data agree with other systems in the literature, thanks to a decrease of the [Si/O] values of these absorbers of $\gtrsim$0.4 dex. The changes in relative abundances are generally due to an overestimate of the Si II column densities in the NIRSpec spectra, possibly deriving from line blending. The only point from Christensen et al. (2023) that remains consistent with an

Table 1
Revised Abundance Ratios for the Systems Reported by Christensen et al. (2023) along the Sight Lines to UHS J0439+1634 and ULAS J1342+0928 Based on the X-Shooter Spectra

QSO	UHS J0439+1634 $z_{abs} = 6.2897$	ULAS J1342+0928 $z_{abs} = 7.36899$	ULAS J1342+0928 $z_{abs} = 7.44345$
[Si/O]	> -0.46	0.10 ± 0.21	-0.03 ± 0.14
[C/O]	> -0.57	-0.20 ± 0.30	-0.58 ± 0.34
[C/Fe]	0.55 ± 0.09	> -0.06	> -0.96
[O/Fe]	<1.12	>0.14	> -0.38
[Si/Fe]	0.66 ± 0.05	>0.24	> -0.41
[Mg/Fe]	0.32 ± 0.04	...	...
[Mg/Si]	-034 ± 0.05	...	...
[Al/Si]	< -0.83	...	...
[Al/Mg]	< -0.49	...	...

enrichment from PISNe is due to the system at $z = 6.5625$ toward VDES J0020-3653, which at present does not have sufficient high-resolution observations to carry out the analysis of absorption lines.

4. Chemical Diagnostics

In this section, we introduce novel diagnostics to pinpoint systems predominantly enriched by PISNe.

4.1. Purely Pop III–Enriched Environments

In Figure 1, we compare the chemical abundance ratios measured in metal-poor absorbers with the predictions of our model for environments *uniquely* polluted by Pop III SNe, i.e., assuming $f_{\rm PopIII} = 1.0$ and varying the mass and explosion energy of Pop III SNe (see Section 2). For reference we also show the predictions for environments polluted by normal Pop II SNe ($f_{\rm PopIII} = 0.01$).

The *chemical diagnostics* presented here were specifically selected to discern the environments enriched by PISNe from other SN types. Indeed, we see that PISN-polluted environments reside in very specific regions of the plots, having quite high $[{\rm Si/O}] > 0.2$, low values of $[{\rm C/O}] < -0.5$ and $[{\rm Al/Si}] < -1.5$, and the lowest values of $[{\rm Al/Mg}] < -1.0$. Thus, the combination of the abundance ratios shown in Figure 1 represents a powerful tool to pinpoint PISN-enriched environments. On the contrary, the environments enriched by the other types of Pop III SNe are not completely separated one from the other and their chemical abundance ratios partially overlap with those imprinted by normal Pop II SNe.

In Figure 1 (top right), we see that only the system toward VDES J0020-3653 in Christensen et al. (2023) remains consistent with an imprint from PISN. Comparing the [Si/O] value of this absorber with the predictions of our model for the environments polluted solely by PISN, we determine the possible initial masses for the PISN that enriched this absorber, $m_* \in [183.0; 234.0]\, M_\odot$. Then, we predict the range of abundances for other elements, which would imply that this absorber was truly and uniquely polluted by PISNe: $[{\rm O/Fe}] \simeq [-0.35; 1.04]$, $[{\rm Al/Si}] \simeq [-2.16; -1.95]$, $[{\rm Si/Fe}] \simeq [0.40; 1.58]$, and $[{\rm Al/Mg}] \simeq [-1.38; -1.28]$.

Finally, we see that the different chemical abundances predicted for Pop III–enriched environments and measured in various absorbers nicely follow the same trends, with several systems overlapping with the predicted abundances in the various chemical diagnostics. Does this mean that all these absorbers have been imprinted by Pop III SNe?

4.2. Pop II Contribution: The Confusion Region

In Figure 2 we show how the injection of heavy elements from Pop II SNe changes the chemical abundances of PISN and other Pop III SN preenriched environments. To this end, we compute the probability density regions of environments solely (100% metals), mainly ($\geqslant$60%), and only partially ($\leqslant$50%) enriched by Pop III (PISNe or other SNe), thus varying $f_{\rm PopIII}$. We see that the contribution of normal Pop II SNe enlarges the regions predominantly imprinted by PISNe, which partially overlap with those mainly enriched by other Pop III/II SNe. Furthermore, while there is still a partial separation between environments mainly polluted by PISNe and by other Pop III SNe, when Pop II SNe become the dominant contributors the two regions almost completely overlap, meaning that we are loosing the information about the pristine SNe that initially enriched these media.

In each diagnostic of Figure 2, we notice the emergence of regions in which the chemical abundance ratios predicted for Pop III (PISNe and other pristine SNe) and Pop II–dominated environments blend. We dub this area the *confusion region*, since environments dwelling in this specific zone might have been imprinted by different sources: one Pop III SN (or two, see Appendix B), a mixture of Pop III and Pop II SNe or a population of normal Pop II SNe. In Figure 2, we see that the majority of the absorption systems present in the literature reside within the confusion regions and in particular, in most of the proposed diagnostics, they are consistent with an enrichment dominated by normal Pop II SNe, but not solely driven by Pop II SNe (see Figure 1). Thus, the nature of the absorbers dwelling in the confusion regions might remain undetermined, even by studying their abundance patterns with the currently available $\leqslant$5 abundance ratios.

To pinpoint PISN- and other Pop III–enriched environments, we should thus look for absorbers that dwell outside of the confusion regions, i.e., in areas where the Pop III chemical fingerprints are preserved. To this end, we see that the odd–even abundance ratios are extremely effective in locating PISN-dominated environments, for example $[{\rm Al/Mg}] < -0.75$ and $[{\rm Al/Si}] < -1.5$ (see also Takahashi et al. 2018). The absorption system at $z = 3.39$ in the spectrum of J1018+0548 from Saccardi et al. (2023; black cross in Figures 1, 2, and 3) lies at $[{\rm Al/Mg}] = -1.23$ and $[{\rm Si/Fe}] = 0.13$ implying that it might be predominantly enriched by PISNe. However, when we consider its positions in other diagnostic plots, we see that this absorber is also consistent with being predominantly enriched by both PISNe and other Pop III SNe.

So far, we have confined our discussion to elements commonly measured in high-z absorbers. However, in nearby stars, we typically measure other elements. For example, for the newly discovered LAMOST star likely imprinted by PISNe (J1010+2358; Xing et al. 2023), it was not possible to measure the abundances of C, O, and Al, while they were determined for many elements heavier than Ca. In Figure 3, we show other four chemical diagnostics for which the star J1010+2358 is always consistent with a PISN-dominated enrichment. Measuring the C (or the Zn) abundance would be fundamental, since a value of $[{\rm C/Fe}] < -1.2$ (or $[{\rm Zn/Fe}] < -1.5$) would imply an exclusive enrichment by PISNe.

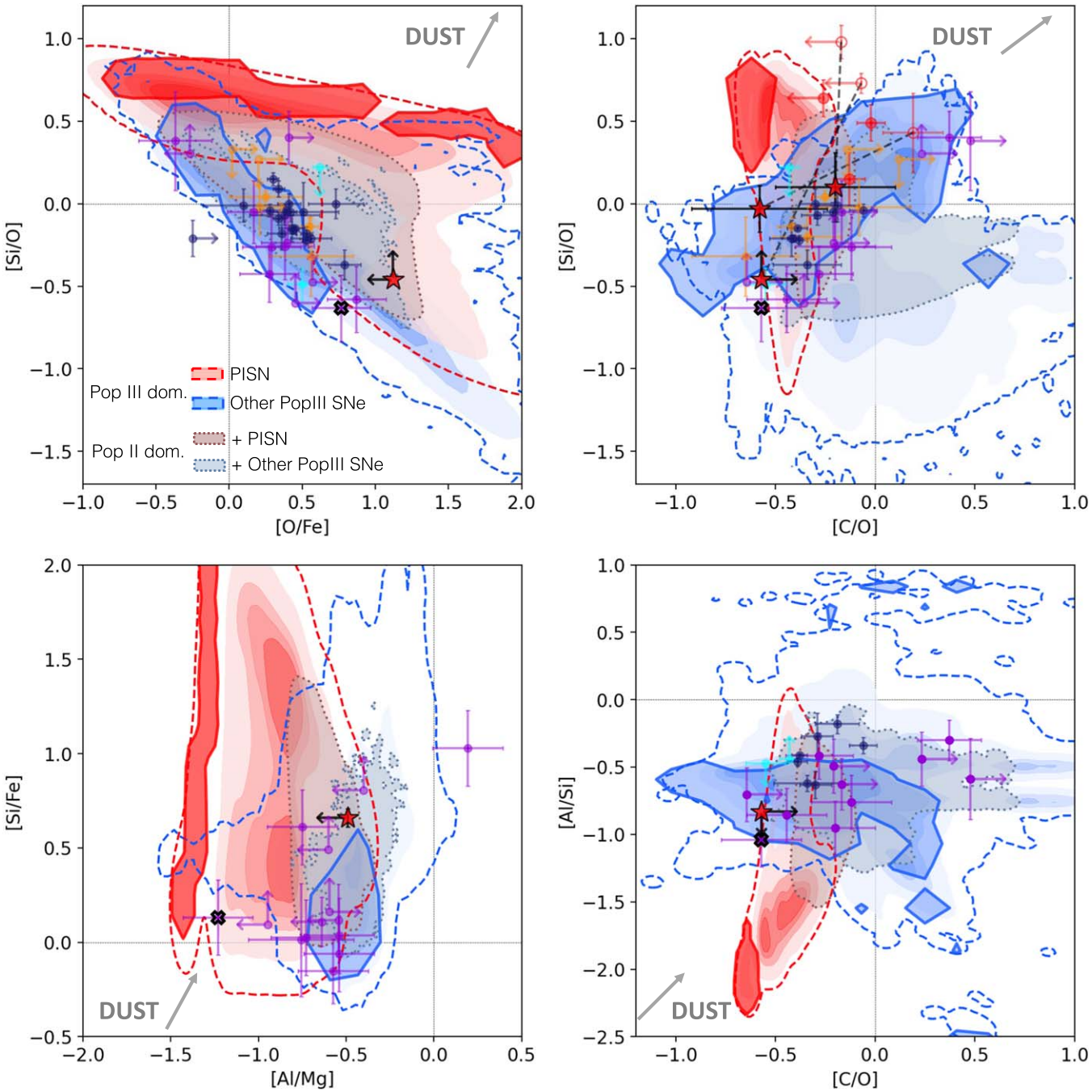

Figure 2. The same as Figure 1 but for environments whose metals have been inherited: uniquely by PISNe/other Pop III SNe (red/blue solid line, $f_{\rm PopIII} = 1$); mainly by PISNe/other Pop III SNe but also by normal Pop II SNe (red/blue dashed lines, $f_{\rm PopIII} \geqslant 0.6$); mainly by normal Pop II SNe but also by PISNe/other Pop III SNe (brown/gray dotted lines, $f_{\rm PopIII} \leqslant 0.5$).

4.3. A Unique Absorber

The absorber J1018+0548 agrees with an enrichment dominated by PISN or other Pop III SNe in all the proposed diagnostics (Figures 2–3). By applying chi-square diagnostics (see Appendix C), we looked for the models that best reproduce its abundance pattern, i.e., with reduced chi square, χ^2_ν, lower than 2 times the minimum one (Figure 4). The minimum $\chi^2_\nu = 0.19$ corresponds to an enrichment driven by two Pop III SNe with equal explosion energy ($E_{\rm SN} = 1.8 \times 10^{51}$ erg) but very different masses (≈10 and 100 $M_\odot$; see Table 3). However, a low $\chi^2_\nu = 0.37$, is also obtained when considering a pollution from a 253 $M_\odot$ PISN (contributing to 10% of the metals), and a ≈30 $M_\odot$ Pop III SN with $E_{\rm SN} = 1.2 \times 10^{51}$ erg. Both models fit very well the abundance ratios of the five light elements measured in the J1018+0548 absorber. However, they strongly differ for elements heavier than Ca, in particular [Zn/Fe], which is ≈1.5 dex lower for massive PISN enrichment.

5. Conclusions

In this Letter, we present novel chemical diagnostics to isolate PISN-enriched environments from those imprinted by

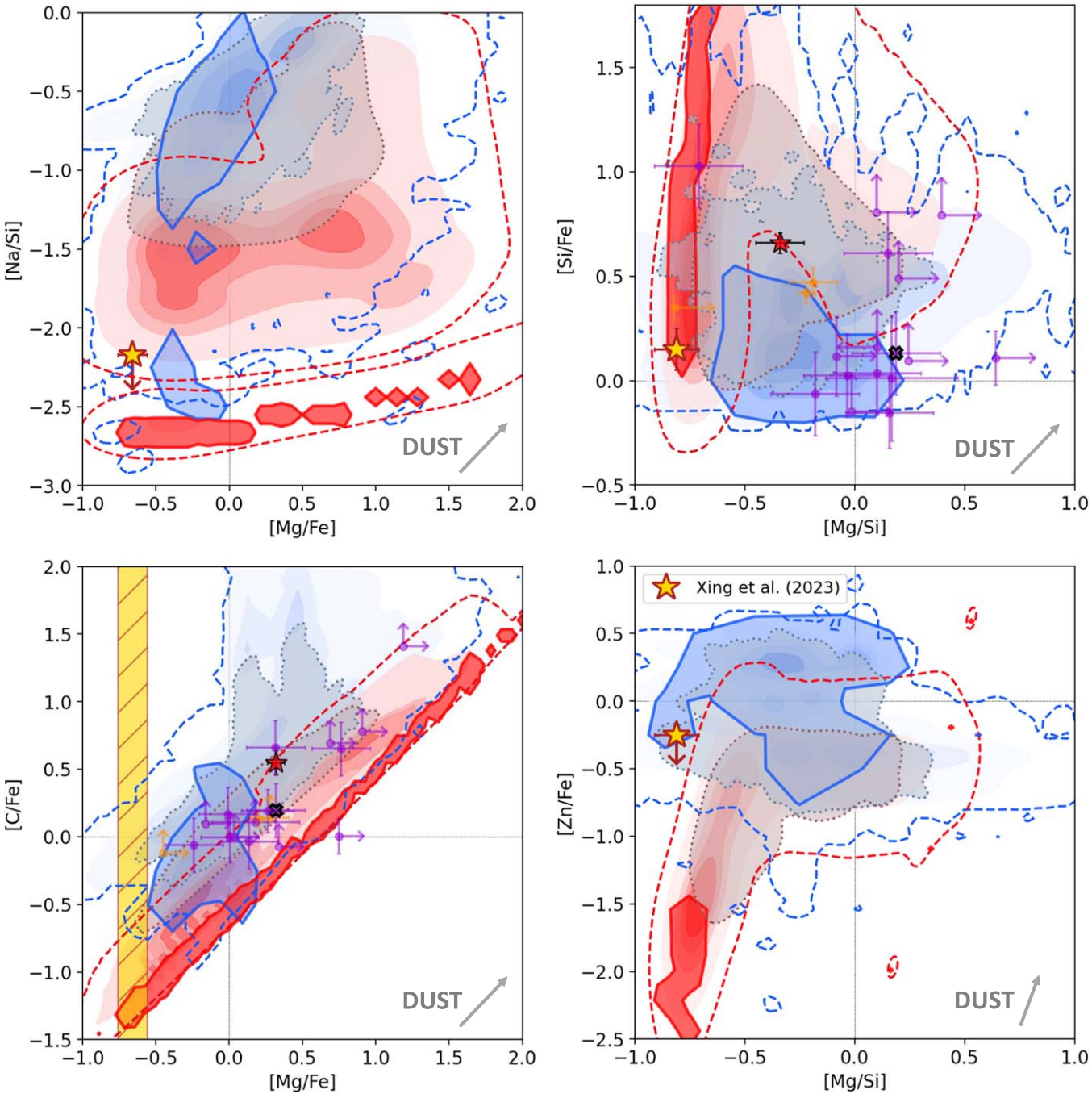

Figure 3. The same as Figure 2. The yellow star and shaded area are the abundances of Xing et al.'s (2023) star: the possible pure PISN descendant.

other Pop III SNe and normal Pop II stars. To this end, we exploited the simple and general parametric model by Vanni et al. (2023b). We show that environments enriched by a single PISN dwell in well defined zones of the proposed chemical diagnostics. Indeed they cover >2 dex in [X/Fe] but have characteristic values of [Al, Mg, Na/Si], and [Si, C/O], covering <0.5 dex. However, when the contribution of normal Pop II SNe is accounted for, regions predominantly imprinted by PISNe ($\geqslant$60% of metals) grow and blend with those mainly enriched by other Pop III or Pop II SNe, creating the so-called confusion regions. Our predictions are very general and thus can be used to interpret the chemical properties of various environments across cosmic times: high-z emitting galaxies (e.g., D'Eugenio et al. 2023), distant gaseous absorbers in the sight line of QSOs or gamma-ray bursts (see also Ma et al. 2017b) and ancient stellar fossils in our Local Group (Vanni et al. 2023b).

By comparing our model predictions with measurements in high-z absorbers, we see that most systems in the literature have elemental abundances consistent with being mainly imprinted by normal Pop II SNe, in agreement with previous studies (e.g., Becker et al. 2012; Salvadori & Ferrara 2012). Note that we do not account for dust depletion since most absorbers in our literature sample are metal-poor, meaning that dust should not affect substantially their chemical abundances (Vladilo et al. 2018; Saccardi et al. 2023). In Figures 1, 2, and

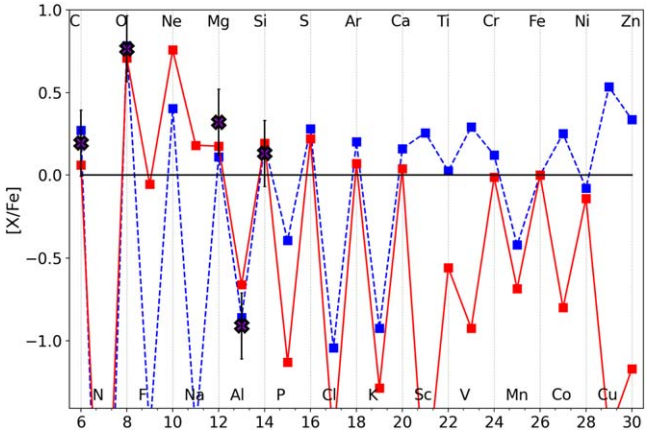

Figure 4. Abundance pattern of the absorber J1018+0548 (Saccardi et al. 2023; black crosses) compared with the two best-fitting models predicting an enrichment from: (i) a PISN and a Pop III SN (red); (ii) two Pop III SNe (blue).

3, we show in which direction the predictions would shift if dust was present, using the prescriptions of Konstantopoulou et al. (2024; see also De Cia et al. 2016).

Our analysis of the publicly available high-resolution X-Shooter spectra for two QSOs presented by Christensen et al. (2023) reconciles the chemical abundances of two absorption systems, suggesting exclusive PISN enrichment, with literature data, i.e., with an enrichment dominated by normal Pop II SNe. Only the system at $z = 6.5625$ along the sight line to VDES J0020-3653, for which high-resolution spectra are not available, remains consistent with a PISN pollution for the three measured elements. Conversely, the Galactic halo star observed at high-resolution by (Xing et al. 2023; 12 elements) is in agreement with an exclusive PISN enrichment in all considered diagnostics. Still, more chemical elements (e.g., C) need to be measured to confirm a pure pollution by a massive PISN (see also Koutsouridou et al. 2024).

Our novel chemical diagnostics allowed us to uncover an absorption system ($z = 3.39$ in J1018+0548; Saccardi et al. 2023) that is consistent with being *uniquely* enriched by Pop III SNe (see Figure 4). Notwithstanding the six chemical elements measured, to understand if this absorber was enriched by a PISN, it is crucial to measure zinc (Section 4.3). The high-resolution spectrograph ANDES for the Extremely Large Telescope (ELT) will allow us to achieve this goal, understanding the nature of this unique absorber (D'Odorico et al. 2023b).

Ultimately, armed with our novel chemical diagnostics and ANDES/ELT, we will be able to unveil these precious distant gas clouds, fully complementing stellar archeology to shed light on the first stars and their role on early galaxy formation.

Acknowledgments

This project received funding from the ERC Starting Grant NEFERTITI H2020/808240 (PI: S. Salvadori). G.D.B. was supported by the National Science Foundation through grant AST-1751404.

Appendix A
Analysis of X-Shooter Quasar Spectra

In this section, we report the results of the fit of three absorption systems discussed in Christensen et al. (2023) for which we analyzed the corresponding X-Shooter spectra.

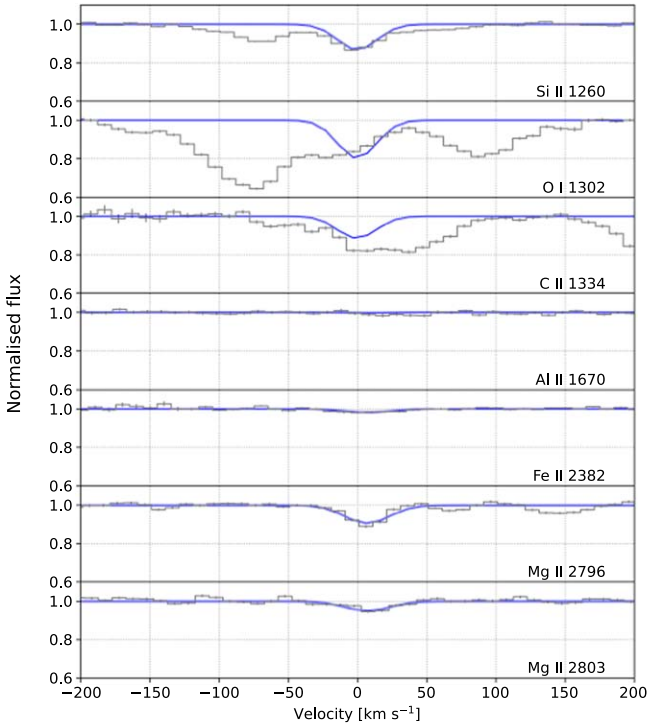

Figure 5. Transitions detected at $z = 6.2897$ in the X-Shooter spectrum of UHS J0439+1634. The observed flux is plotted as a gray histogram with 1σ error bars plotted for each pixel; the Voigt profile model is plotted as a blue solid line. This figure can be compared with Figure B.45 in Christensen et al. (2023), noting the different velocity scale.

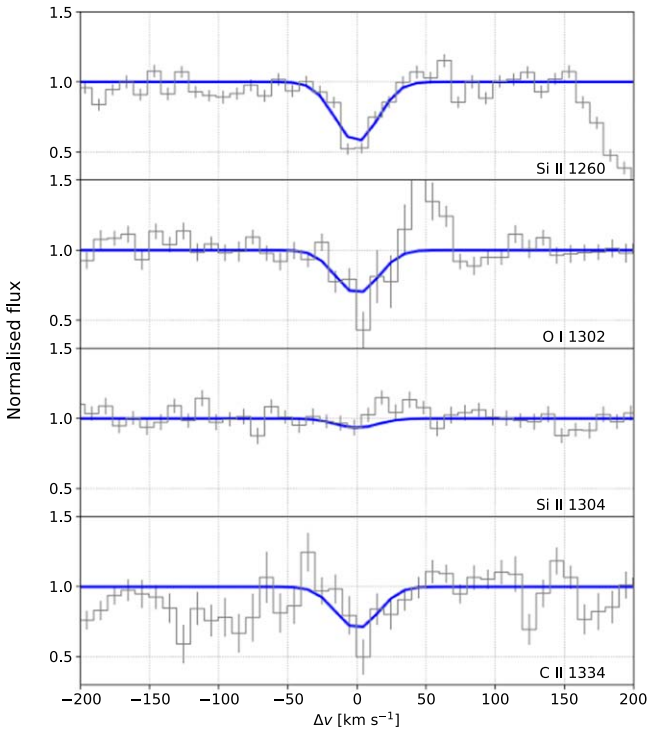

Figure 6. Transitions detected at $z = 7.368$ in the X-Shooter spectrum of ULAS J1342+0928. The lines are the same as in Figure 5. This figure can be compared with Figure B.59 in Christensen et al. (2023), noting the different velocity scale.

The spectrum of UHS J0439+1634 is the one released by the XQR-30 collaboration (D'Odorico et al. 2023b), while the spectrum of ULAS J1342+0928 was reduced and analyzed in

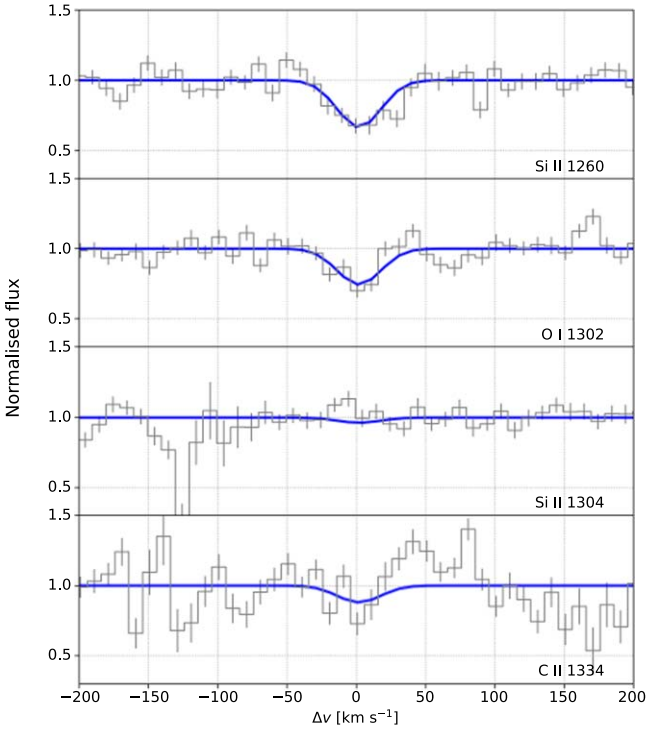

Figure 7. Transitions detected at $z = 7.4434$ in the X-Shooter spectrum of ULAS J1342+0928. The lines are the same as in Figure 5. This figure can be compared with Figure B.60 in Christensen et al. (2023), noting the different velocity scale.

Table 2
Column Densities for the Systems Reported by Christensen et al. (2023) along the Sight Lines to UHS J0439+1634 and ULAS J1342+0928 Determined in the X-Shooter Spectra

QSO	UHS J0439+1634	ULAS J1342+0928	ULAS J1342+0928
z_{abs}	6.2897	7.36899	7.44345
b (km s^{-1})	16 ± 2	8	8
C II	13.03 ± 0.08	13.57 ± 0.23	13.07 ± 0.33
O I	<13.86	14.03 ± 0.19	13.91 ± 0.1
Si II	12.22 ± 0.03	12.95 ± 0.10	12.70 ± 0.10
Mg II	11.97 ± 0.05	...	...
Al II	<10.33	...	...
Fe II	11.55 ± 0.04	<12.70	<13.10

this work. Briefly, ULAS J1342+0928 was observed with VLT/X-Shooter in 2017 and 2018 (PID 098.B-0537, 0100.A-0898) for ~23 hr adopting a slit of 0.″6 in the Near-Infrared (NIR) arm. We retrieved the raw frames from the ESO archive and reduced them with the custom pipeline described in D'Odorico et al. (2023b). The combined spectrum has a nominal resolving power $R \simeq 8100$ and a signal-to-noise ratio S/N ≃19 per 10 km s^{-1} bin at $\lambda = 1285$ Å rest frame. This value, converted to the JWST/NIRSpec wavelength bin at $\lambda \sim 1.1$ μm ($\Delta v \simeq 64$ km s^{-1}) increases to S/N ≃ 50, comparable to the one of the spectra analyzed by Christensen et al. (2023; S/N ≈ 60; see their Figure 5).

The absorption lines have been fitted with Voigt profiles using the Python package Astrocook (Cupani et al. 2022). For the three analyzed systems, we assumed that the Doppler parameters were the same for all observed transitions. In the case of the two systems along the spectrum of ULAS J1342+0928, we fixed the Doppler parameter to the minimum value allowed by the resolving power of the observations (see Sodini et al. 2024). However, we checked that decreasing the Doppler parameter to 6 km s^{-1} the results do not change significantly. Due to the limited NIR coverage of the X-Shooter spectrum with respect to the NIRSpec one, we do not cover the Mg II doublet transitions for either system.

In the case of the system at $z = 6.2897$ in the spectrum of UHS J0439+1634, Christensen et al. (2023) identify as O I 1302 Å at $z = 6.288$ an absorption feature which Davies et al. (2023) fit in the X-Shooter spectrum as a C IV doublet at $z = 5.1299$. For the purpose of this Letter and in order to compare with the results by Christensen et al. (2023), we derived a conservative upper limit on the O I column density fitting the observed absorption assuming the redshift and the Doppler parameter of the Si II 1260 Å absorption line of this system, i.e., assuming $z \approx 6.2897$. The very good quality of the X-Shooter spectrum allowed us also to measure the column density of a very weak Fe II 2382 Å absorption line and to determine an upper limit to the transition of Al II 1670 Å. The absorption lines and the Voigt profile fit for the three studied systems are shown in Figures 5, 6, and 7, while the measured column densities are reported in Table 2.

Appendix B
Environments Enriched by a PISN and Another Pop III SN

Cosmological simulations predict that the first stars formed preferentially isolated, but they could also appear in small groups (see, e.g., Skinner & Wise 2020). Furthermore, in this work we aim at providing chemical diagnostics to study the fingerprints of the first stars in distant absorbers, including Lyman Limit systems and sub-DLAs. The nature of these systems is still unclear and they might be associated to gaseous filaments enriched by different low-mass galaxies hosting Pop III stars. For these reasons, in this section we investigate how the chemical diagnostics for PISN-enriched environments are affected when considering the contribution of a second Pop III SN, i.e., further exploring the case $f_{\rm PopIII} = 1$.

The results of our investigation are shown in Figures 8–9, where we compare the chemical abundance ratios predicted for environments enriched by one PISN and another Pop III SN (i.e., two Pop III SNe and $f_{\rm PopIII} = 1$) with those previously shown in Figures 2–3. Clearly, these abundance ratios are widespread in our chemical diagnostics, covering the areas predicted for environments enriched by single PISNe, other Pop III SNe, and a mixture of PISNe and Pop II SN, i.e., the so-called confusion regions. Thus, absorbers in the confusions regions might be enriched by Pop III only ($f_{\rm PopIII} = 1$) through a combination of a PISN and another Pop III SN, or predominantly enriched by a populations of normal Pop II SNe ($f_{\rm PopIII} \leqslant 0.5$). To uncover the nature of these absorbers, we should use all the proposed diagnostics and, eventually, use a χ^2 fitting procedure (see Appendix C) exploiting their overall abundance pattern.

It is important to note that in all our diagnostics the absorber J1018+0548 (black cross) is consistent for being enriched by a PISN and another Pop III SN, i.e., uniquely imprinted by Pop III stars. To unveil the properties of their progenitors, we need to compare its observed chemical abundance pattern with our theoretical predictions as we will explain in the next section.

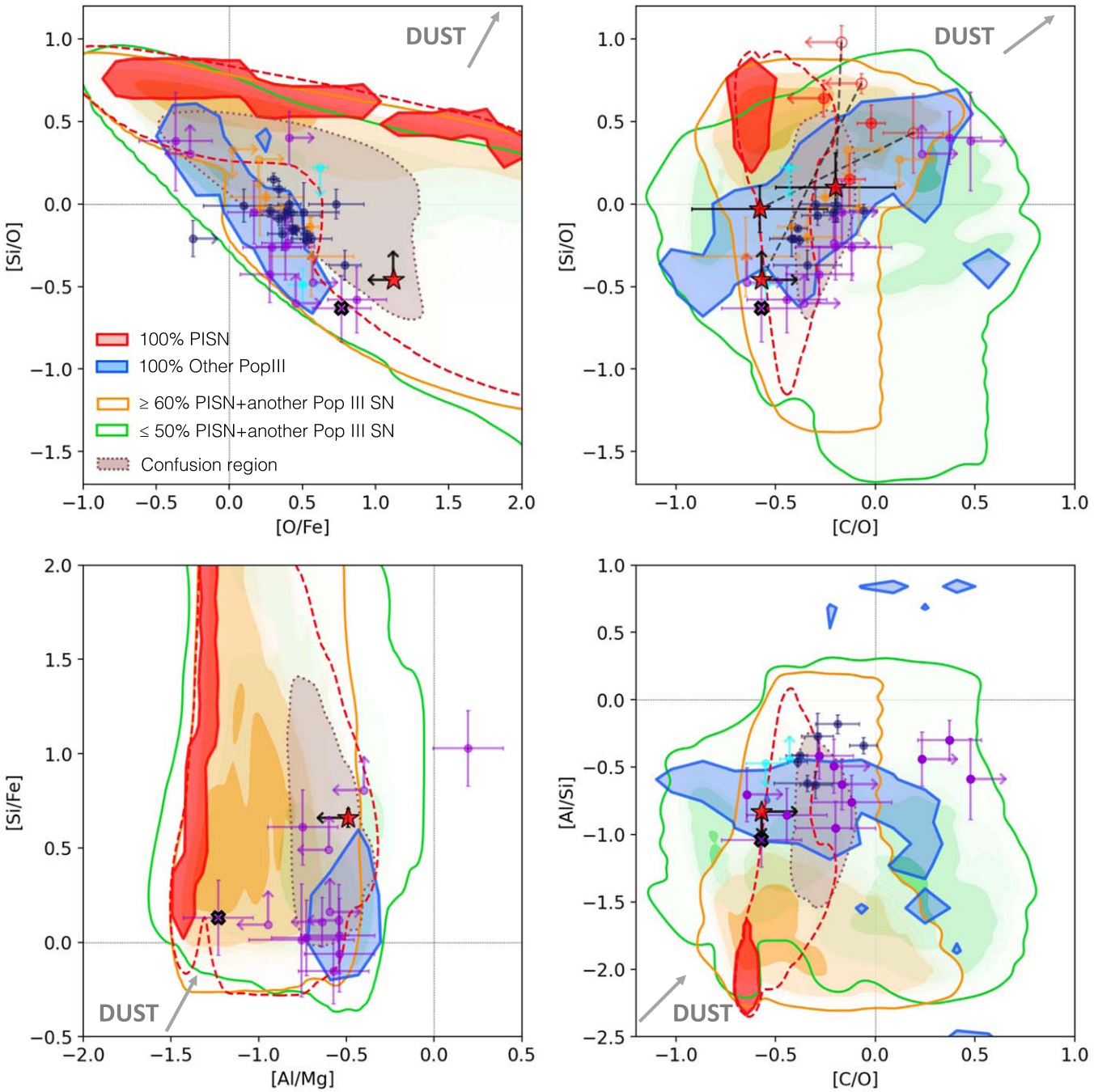

Figure 8. Same as Figure 2, but the chemical abundances are inherited by only PISNe (solid red), only other Pop III SNe (solid blue), and a single PISN but also another Pop III SN in different proportions (≥60% PISN: solid orange; ≤50% PISN: solid green). We show also the chemical abundances predicted for environments enriched mainly by PISNe but also by Pop II SNe ($f_{\rm PopIII} \geqslant 0.6$, dashed red) and mainly by Pop II SNe but also by PISNe ($f_{\rm PopIII} \leqslant 0.5$, dotted gray; see Figures 2–3).

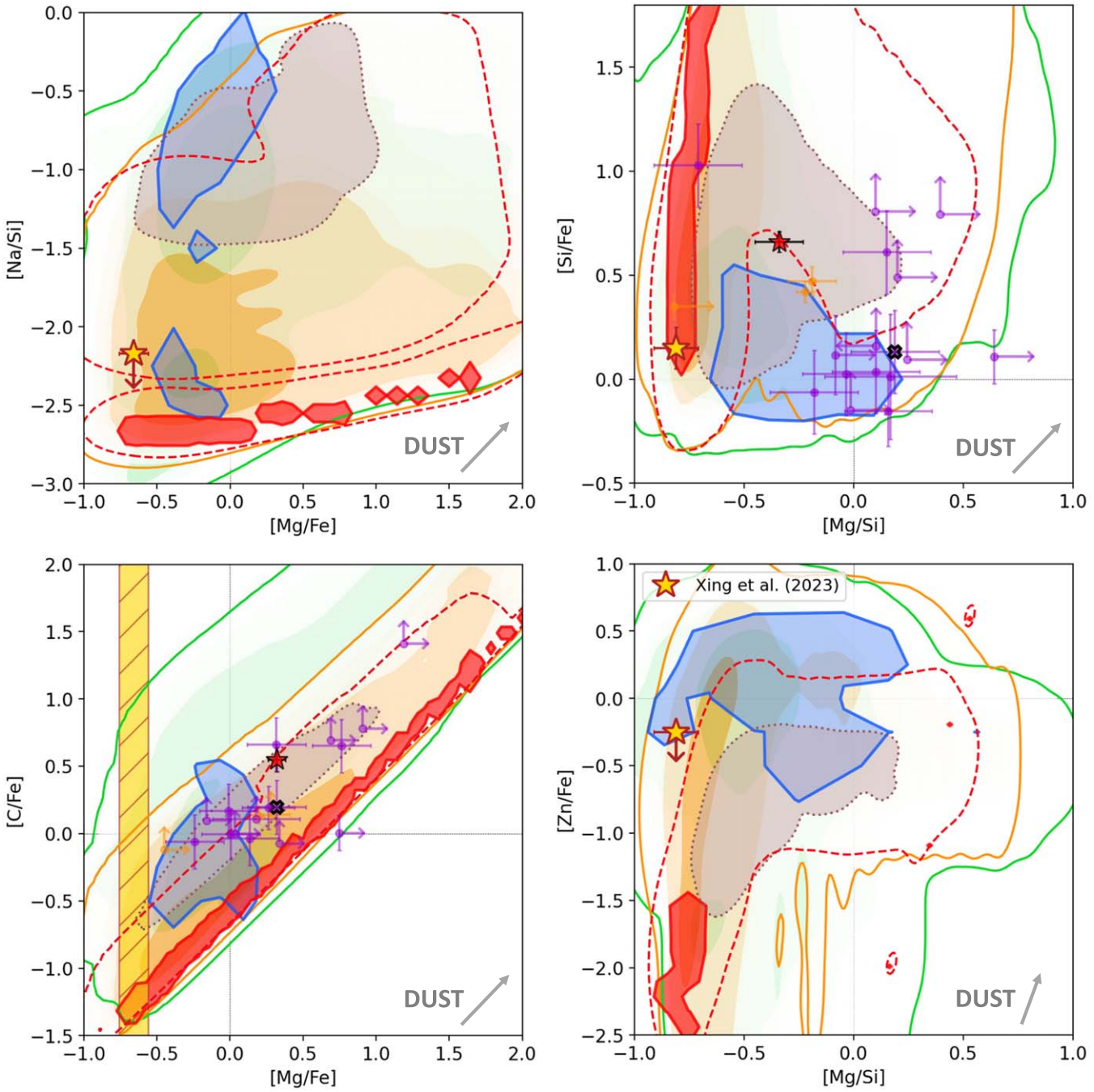

Figure 9. The same as Figure 3, but with the additional models described in the caption of Figure 8.

Appendix C
Fitting Procedure

The χ^2 is computed following the equation proposed by Heger & Woosley (2010), which is general and allows us to include the contribution of upper/lower limit measurements in the calculation:

$$\chi^2 = \sum_{i=1}^{N} \frac{(O_i - T_i)^2}{\sigma_{O_i}^2 + \sigma_{T_i}^2} + \sum_{i=N+1}^{N+U} \frac{(O_i - T_i)^2}{\sigma_{T_i}^2} \times \Theta(O_i - T_i) + \sum_{i=N+U+1}^{N+U+L} \frac{(O_i - T_i)^2}{\sigma_{T_i}^2} \times \Theta(T_i - O_i), \quad \text{(C1)}$$

where O_i and T_i are the observed and theoretically predicted abundance ratios [X_i/Fe] and σ_{O_i,T_i} are their respective errors. In order to account for the uncertainties on the stellar yields, we assume $\sigma_{T_i} = 0.50$, as suggested by Nomoto et al. (2013) and Hartwig et al. (2018). $\Theta(x)$ is the Heaviside function. The reduced chi square, χ^2_ν, is computed as $\chi^2/(N+L+U-M)$, where N is the number of data points with finite measurements, L (U) is the number of data points with lower (upper) limits, and M is the number of free parameters of the model (M = 4 with fixed mixing parameter of Pop III SNe). Finally, we define the relative chi square as $\chi^2_{\rm rel} := \chi^2_\nu / min(\chi^2_\nu)$.

To find the best model for the enrichment of the absorption system at $z = 3.39$ in the sight line of the QSO J1018+0548

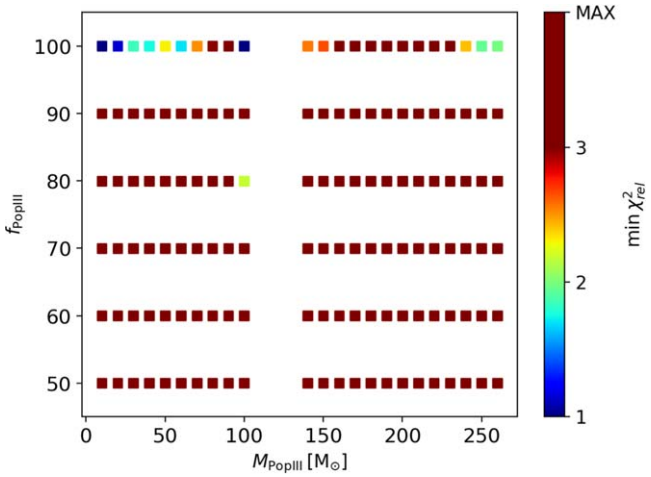

Figure 10. Minimum relative reduced chi square computed fitting the abundances of J1018+0548 for models with different $f_{\rm PopIII}$ and different initial masses of the SN that explodes first, $M_{\rm PopIII}$ or M_1.

Table 3
Parameters of the Best-fitting Models of J1018+0548 Shown in Figure 4

χ^2_ν	$f_{\rm PopIII}$	M_1 ($M_\odot$)	E_1 (10^{51} erg)	M_2 ($M_\odot$)	E_2 (10^{51} erg)	f_1
0.19	1.0	100.0	1.8	11.8	1.8	0.8
0.37	1.0	253.0	97.3	27.5	1.2	0.1

Note. $M_{1,2}$ and $E_{1,2}$ are the initial masses and SN explosion energies of the two Pop III stars polluting the environment. We indicate with f_1 the fraction of metals provided by the Pop III SN that explodes first. Thus, the fraction of metals contributed by the second SN can be computed as $f_2 = 1 - f_1$.

(Saccardi et al. 2023), we look for the minimum χ^2_ν by considering all the models presented in Section 2 (see Figures 1, 2, and 3), i.e., by accounting for an enrichment (i) uniquely driven by a single PISN or a Pop III SN with different mass/energy; (ii) mainly ($\geqslant$60% metals) driven by a single PISN/other Pop III SN with the contribution of Pop II SNe; (iii) only partially ($\leqslant$50% metals) driven by a single PISN/other Pop III SN with the contribution of Pop II SNe. Furthermore, we also consider an imprint from two Pop III SNe with various masses and energies, including PISNe, with $f_{\rm PopIII} = 1$ (i.e., excluding the contribution of Pop II SNe). As shown in Figure 4, these models provide the best fits for the abundance pattern of J1018+0548.

In Table 3, we present the parameters of the models displayed in Figure 4, which correspond to an enrichment driven by (i) two Pop III SNe with same explosion energy, $E_{1,2} = 1.8 \times 10^{51}$ erg, but very different masses, $M_1 = 100\,M_\odot$ and $M_2 = 11.8\,M_\odot$ ($\chi^2_\nu = 0.19$); (ii) a very massive PISN of $M_1 = 253\,M_\odot$ and a second Pop III SN with lower mass, $M_2 = 27.5\,M_\odot$, and lower explosion energy, $E_2 = 1.2 \times 10^{51}$ erg ($\chi^2_\nu = 0.37$). The parameter f_1 in the table represents the fraction of metals provided by the Pop III SN/PISN that explodes first, while the fraction contributed by the second one will be $f_2 = 1 - f_1$.

In Figure 10 we show the minimum $\chi^2_{\rm rel}$ obtained by studying all models with different $f_{\rm PopIII}$ and mass of the SN that explodes first, $M_{\rm PopIII}$, regardless of all the other parameters, i.e., E_1, M_2, E_2, f_1, $M_{\rm PopII}$. The chi square shown for models with $f_{\rm PopIII} = 1$ can be either for environments enriched by single Pop III SNe with $M = M_{\rm PopIII}$ or multiple Pop III SNe, where the first SN that explodes has $M_1 = M_{\rm PopIII}$.

We can clearly see in the figure that all models with $f_{\rm PopIII} < 1$ have $\chi^2_{\rm rel} > 3$, apart from a specific model with $f_{\rm PopIII} = 0.8$ (providing $\chi^2_{\rm rel} = 2.21$, $\chi^2 = 0.45$) that describes the combined pollution by a single Pop III SN with $M = 100 M_\odot$ and a normal core-collapse Pop II SN with $M = 13 M_\odot$. Thus, we can safely exclude that the absorber J1018+0548 has been predominantly imprinted by Pop II SNe. As shown in the attached figure, the models with the lowest $\chi^2_{\rm rel}$ are the ones with $f_{\rm PopIII} = 1$, i.e., those uniquely polluted by Pop III SNe: both PISNe+Pop III SNe and two Pop III SNe. We chose to show in Figure 4 the abundance patterns of the best models of these two categories, i.e., models that have $\chi^2_{\rm rel} \leqslant 2$ and that account for an enrichment by two Pop III SNe or by one PISN and a Pop III SN.

ORCID iDs

Irene Vanni https://orcid.org/0000-0001-9647-0493
Stefania Salvadori https://orcid.org/0000-0001-7298-2478
Valentina D'Odorico https://orcid.org/0000-0003-3693-3091
George D. Becker https://orcid.org/0000-0003-2344-263X
Guido Cupani https://orcid.org/0000-0002-6830-9093

References

Aguado, D. S., Salvadori, S., Skúladóttir, Á., et al. 2023, MNRAS, 520, 866
Asplund, M., Grevesse, N., Sauval, A. J., & Scott, P. 2009, ARA&A, 47, 481
Barkat, Z., Rakavy, G., & Sack, N. 1967, PhRvL, 18, 379
Becker, G. D., Sargent, W. L. W., Rauch, M., & Carswell, R. F. 2012, ApJ, 744, 91
Bromm, V., Ferrara, A., Coppi, P. S., & Larson, R. B. 2001, MNRAS, 328, 969
Caffau, E., Lombardo, L., Mashonkina, L., et al. 2023, MNRAS, 518, 3796
Christensen, L., Jakobsen, P., Willott, C., et al. 2023, A&A, 680, A82
Cooke, R., Pettini, M., Steidel, C. C., Rudie, G. C., & Nissen, P. E. 2011, MNRAS, 417, 1534
Cupani, G., D'Odorico, V., Cristiani, S., et al. 2022, in ASP Conf. Ser. 532, ed. J. E. Ruiz, F. Pierfedereci, & P. Teuben (San Francisco, CA: ASP), 207
Davies, R. L., Ryan-Weber, E., D'Odorico, V., et al. 2023, MNRAS, 521, 289
De Cia, A., Ledoux, C., Mattsson, L., et al. 2016, A&A, 596, A97
D'Eugenio, F., Maiolino, R., Carniani, S., et al. 2023, arXiv:2311.09908
D'Odorico, V., Bolton, J. S., Christensen, L., et al. 2023a, arXiv:2311.16803
D'Odorico, V., Bañados, E., Becker, G. D., et al. 2023b, MNRAS, 523, 1399
Frebel, A., Ji, A. P., Ezzeddine, R., et al. 2019, ApJ, 871, 146
Hartwig, T., Yoshida, N., Magg, M., et al. 2018, MNRAS, 478, 1795
Heger, A., & Woosley, S. E. 2002, ApJ, 567, 532
Heger, A., & Woosley, S. E. 2010, ApJ, 724, 341
Hirano, S., Hosokawa, T., Yoshida, N., Omukai, K., & Yorke, H. W. 2015, MNRAS, 448, 568
Hirano, S., Hosokawa, T., Yoshida, N., et al. 2014, ApJ, 781, 60
Ishigaki, M. N., Tominaga, N., Kobayashi, C., & Nomoto, K. 2018, ApJ, 857, 46
Jeena, S. K., Banerjee, P., & Heger, A. 2024, MNRAS, 527, 4790
Klessen, R. S., & Glover, S. C. O. 2023, ARA&A, 61, 65
Kobayashi, C. 2012, in ASP Conf. Ser. 458, Galactic Archaeology: Near-Field Cosmology and the Formation of the Milky Way, ed. W. Aoki et al. (San Francisco, CA: ASP), 113
Konstantopoulou, C., De Cia, A., Ledoux, C., et al. 2024, A&A, 681, A64
Koutsouridou, I., Salvadori, S., Skúladóttir, Á, et al. 2023, MNRAS, 525, 190
Koutsouridou, I., Salvadori, S., & Skúladóttir, Á 2024, ApJL, 962, L26
Limongi, M., & Chieffi, A. 2018, ApJS, 237, 13
Ma, Q., Maio, U., Ciardi, B., & Salvaterra, R. 2017a, MNRAS, 472, 3532
Ma, Q., Maio, U., Ciardi, B., & Salvaterra, R. 2017b, MNRAS, 466, 1140
Nomoto, K., Kobayashi, C., & Tominaga, N. 2013, ARA&A, 51, 457
Pallottini, A., Ferrara, A., Gallerani, S., Salvadori, S., & D'Odorico, V. 2014, MNRAS, 440, 2498

Ritter, J. S., Safranek-Shrader, C., Gnat, O., Milosavljević, M., & Bromm, V. 2012, ApJ, 761, 56
Rossi, M., Salvadori, S., & Skúladóttir, Á 2021, MNRAS, 503, 6026
Rossi, M., Salvadori, S., Skúladóttir, Á, & Vanni, I. 2023, MNRAS, 522, L1
Saccardi, A., Salvadori, S., D'Odorico, V., et al. 2023, ApJ, 948, 35
Salvadori, S., Bonifacio, P., Caffau, E., et al. 2019, MNRAS, 487, 4261
Salvadori, S., D'Odorico, V., Saccardi, A., Skúladóttir, Á, & Vanni, I. 2023, MmSAI, 94, 215
Salvadori, S., & Ferrara, A. 2012, MNRAS, 421, L29
Skúladóttir, Á, Salvadori, S., Amarsi, A. M., et al. 2021, ApJL, 915, L30
Skúladóttir, Á, Vanni, I., Salvadori, S., & Lucchesi, R. 2024, A&A, 681, A44
Skinner, D., & Wise, J. H. 2020, MNRAS, 492, 4386
Smith, B. D., Wise, J. H., O'Shea, B. W., Norman, M. L., & Khochfar, S. 2015, MNRAS, 452, 2822
Sodini, A., D'Odorico, V., Salvadori, S., et al. 2024, arXiv:2404.10722
Susa, H., Hasegawa, K., & Tominaga, N. 2014, ApJ, 792, 32
Takahashi, K. 2018, ApJ, 863, 153
Takahashi, K., Yoshida, T., & Umeda, H. 2018, ApJ, 857, 111
Vanni, I., Salvadori, S., & Skúladóttir, Á 2023a, MmSAI, 94, 84
Vanni, I., Salvadori, S., Skúladóttir, Á, Rossi, M., & Koutsouridou, I. 2023b, MNRAS, 526, 2620
Vladilo, G., Gioannini, L., Matteucci, F., & Palla, M. 2018, ApJ, 868, 127
Welsh, L., Cooke, R., Fumagalli, M., & Pettini, M. 2022, ApJ, 929, 158
Welsh, L., Cooke, R., & Fumagalli, M. 2019, MNRAS, 487, 3363
Xing, Q.-F., Zhao, G., Liu, Z.-W., et al. 2023, Natur, 618, 712